

Titanium dioxide nanoswords with highly reactive, photocatalytic facets

This article has been downloaded from IOPscience. Please scroll down to see the full text article.

2010 Nanotechnology 21 485601

(<http://iopscience.iop.org/0957-4484/21/48/485601>)

View [the table of contents for this issue](#), or go to the [journal homepage](#) for more

Download details:

IP Address: 169.229.32.137

The article was downloaded on 12/11/2010 at 20:21

Please note that [terms and conditions apply](#).

Titanium dioxide nanoswords with highly reactive, photocatalytic facets

Brian D Sosnowchik¹, Heather C Chiamori¹, Yong Ding²,
Jong-Yoon Ha¹, Zhong Lin Wang² and Liwei Lin^{1,3}

¹ Department of Mechanical Engineering and Berkeley Sensor and Actuator Center 497 Cory Hall, University of California at Berkeley, Berkeley, CA 94720, USA

² School of Materials Science and Engineering, Georgia Institute of Technology, 771 Ferst Dr., Atlanta, GA 30332, USA

E-mail: bdsnow@me.berkeley.edu, chiamori@berkeley.edu, yong.ding@mse.gatech.edu, jongyoon@me.berkeley.edu, zhong.wang@mse.gatech.edu and lwlin@me.berkeley.edu

Received 25 August 2010

Published 8 November 2010

Online at stacks.iop.org/Nano/21/485601

Abstract

Titanium dioxide (TiO₂) is one of the most widely studied and important materials for catalysis, photovoltaics, and surface science applications, but the ability to consistently control the relative exposure of higher surface energy facets during synthesis remains challenging. Here, we present the repeatable synthesis of highly reactive, rutile {001} or {101} facets on broad, sword-shaped TiO₂ nanostructures rapidly synthesized in minutes. Growth occurs along planes of lower surface energy, repeatedly yielding nanostructures with large, high energy facets. The quantitative photocatalytic reactivity of the nanoswords, demonstrated by the photoreduction of silver, is over an order of magnitude higher than reference low energy TiO₂{110} substrates. Therefore, the higher surface energy dominated TiO₂ nanoswords are ideal structures for characterizing the physicochemical properties of rutile TiO₂, and may be used to enhance a variety of catalytic, optical, and clean-technology applications.

 Online supplementary data available from stacks.iop.org/Nano/21/485601/mmedia

(Some figures in this article are in colour only in the electronic version)

1. Introduction

The physicochemical properties of a material are strongly dependent on the crystallographic orientation, surface structure, and free energy of the material [1–6]. While surfaces of high reactivity are critically important for specific applications, often the surfaces resulting from crystallographic growth favor those with lower free energy facets [7, 8]. Because of this, it is highly desirable to reliably engineer predictable, high surface energy, reactive facets for applications necessitating largely expedited or enhanced surface reactions. Titanium dioxide (TiO₂) is the most investigated metal oxide because of its unique surface properties [3], but equilibrium rutile and anatase phase TiO₂ single crystal nanoparticles are dominated by low surface energy {110} and {101} facets, respectively [7, 9]. Of the low index anatase surfaces, the {001} facet has the highest surface energy [10], and recently, several groups have

demonstrated the ability to synthesize particles with a large percentage of {001} facets [2, 11] and improved photocatalytic performance [12]. For low index rutile surfaces, the {101} and {001} facets have the highest surface energies [7, 13], with interestingly, the theoretical surface energy values of the rutile {101} surface exceeding those of anatase {001} for many surface conditions [8, 9]. Here, we demonstrate a rapid, simple, and dry chemical vapor growth process to synthesize rutile TiO₂ nanostructures with a distinctively unique shape yielding large, highly reactive {001} or {101} facets and ultrasharp tips. The large-scale synthesis process is accomplished in a matter of minutes, repeatedly yielding nanoswords with a well-defined geometry, comprising a naturally forming structure, over 90% of which exposes high free energy surfaces. This large percentage of highly reactive surfaces on the nanoswords represents a more than 3.5-fold increase over the equilibrium rutile crystal [7], and the photocatalytic activity of the nanoswords, demonstrated through the reduction of silver,

³ Author to whom any correspondence should be addressed.

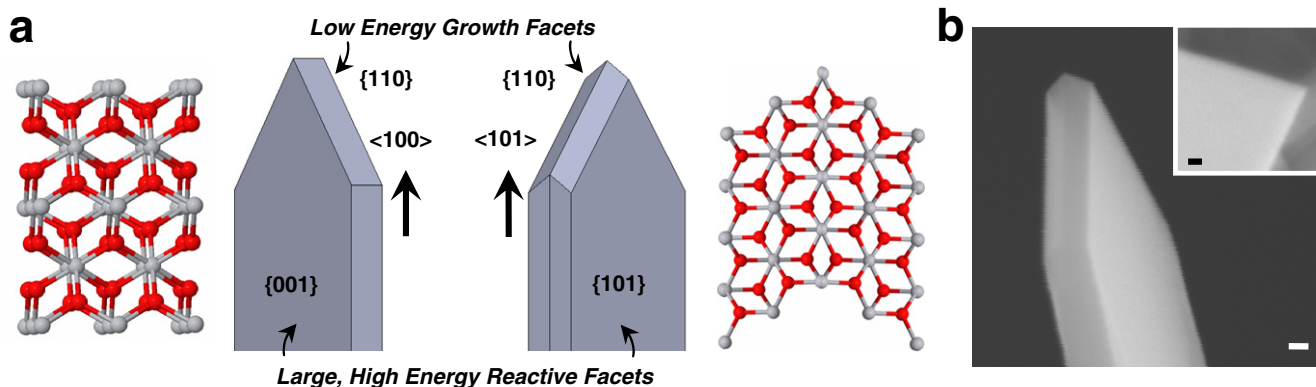


Figure 1. Schematic illustrations and electron micrographs of rapidly synthesized TiO_2 nanoswords. Schematic orientations and atomic structures of the two rutile nanoswords synthesized in this work are shown in (a). The growth front of the rutile nanoswords is defined by lower energy $\{110\}$ planes and the large surfaces are higher energy $\{001\}$ and $\{101\}$ planes. (b) Scanning electron micrographs reveal a broad and flat nanostructure with taper and tip angles that are coplanar and perpendicular to the large facet, respectively. The nanoswords may be synthesized in large quantity and have ultrasharp tips, as shown in the inset. Scale bars for (b) and the inset are 50 nm and 20 nm, respectively.

was observed to be over an order of magnitude higher than reference (110) substrates.

High temperature vapor–liquid–solid (VLS) and vapor–solid (VS) processes have been used to synthesize nanotubes, nanowires, and nanobelts [14–16]. The high temperature environment promotes the energetic movement of molecules for one-dimensional growth. For example, very long (up to a few millimeters) semiconducting oxide nanobelts, including ZnO , SnO_2 , Ga_2O_3 , In_2O_3 , CdO , and PbO_2 have been synthesized [15]. Frequently, the growth occurs at high surface energy sites resulting in nanobelts or nanowires with low free energy surfaces [17]. However, in certain instances, kinetically favorable growth conditions promote the synthesis of nanobelts with high free energy surfaces [18], and such phenomena provide a unique way to expose facets of higher reactivity that were not previously achievable.

Here, the epitaxial formation of thermodynamically lower energy surfaces—the $\{110\}$ in the rutile phase [3]—are the growth-front leading surfaces during the formation of single crystal nanoswords with broad, highly reactive facets. The schematic representations, atomic structures, and synthesized structures in figures 1(a) and (b) summarize the two nanoswords synthesized in this work. The first type grows along the $\langle 100 \rangle$ direction, enclosed by two $\{110\}$ facets, resulting in a broad, more reactive $\{001\}$ surface, while the second type grows along the $\langle 101 \rangle$, enclosed by four $\{110\}$ facets, resulting in the exposure of $\{101\}$ facets. These nanoswords have the unique combined properties of having a high surface-to-volume ratio, ultrasharp tip (inset of figure 1(b)), a high percentage of reactive surfaces, and may be densely grown in a large scale for a wide range of potential applications in photovoltaics, the photolyzing of water, cosmetics, clean-tech, photocatalysts, and optics, to name a few.

2. Results and discussion

Various processes have been previously reported for the synthesis of one-dimensional TiO_2 nanostructures, and there

are several common disadvantages. In general, the synthesis times remain relatively long (30 min to three days in some cases [19]), and the resulting nanostructures from sol–gel templating [20, 21], without templates [22, 23], and via physical vapor deposition [24], are of low quality without well-defined, highly reactive facets. In contrast, our synthesis process is based on an induction heating platform that is easy to set up, clean, inexpensive, and enables synthesis in minutes [25, 26]. A 50–350 nm thin film of titanium is evaporated on top of a conductive substrate as the source material. The samples are placed at the center of an induction heating coil (Novastar 1 M, Ameritherm Inc.) in a custom-made quartz chamber, where temperature, gas pressure, and processing time are controlled (see supplementary data available at stacks.iop.org/Nano/21/485601/mmedia). Power is initiated to rapidly elevate the substrate temperature to a desired value between 850 and 950 °C, thereby enabling the vapor–solid synthesis of the nanoswords.

A detailed analysis by transmission electron microscopy (TEM) of the two types of TiO_2 nanoswords is presented in figure 2. The characteristic surfaces and orientations of each nanosword are highlighted schematically in figure 2(a), illustrating both single crystal (type I) and twinned (type II) nanoswords. Figure 2(b) shows a high-resolution TEM image of a type I single crystal nanosword. The distance between the lattice planes was measured to be 4.6 Å, corresponding to the d -spacing of adjacent $\{100\}$ planes (JCPDS card 21-1276). The ultrasharp tip may also be observed in figure 2(b), with a radius of curvature of ~ 2 nm. Its selected-area electron diffraction (SAED) pattern is shown in figure 2(c), which can be indexed with the incident beam along the $[001]$ direction. The comparably weak contrast of the four diffraction spots, (100) , $(\bar{1}00)$, (010) , $(0\bar{1}0)$ are due to the existence of a screw axis 4_2 in the rutile structure (space group of $P4_2mnm$). The large top and bottom surfaces of these nanoswords belong to $\{001\}$ planes, and its tip is terminated by two inclined $\{110\}$ planes, creating a 90° taper angle projected along the $[001]$ direction.

The twin plane in the side view of a type II nanosword is clearly visible in the TEM image shown in figure 2(d),

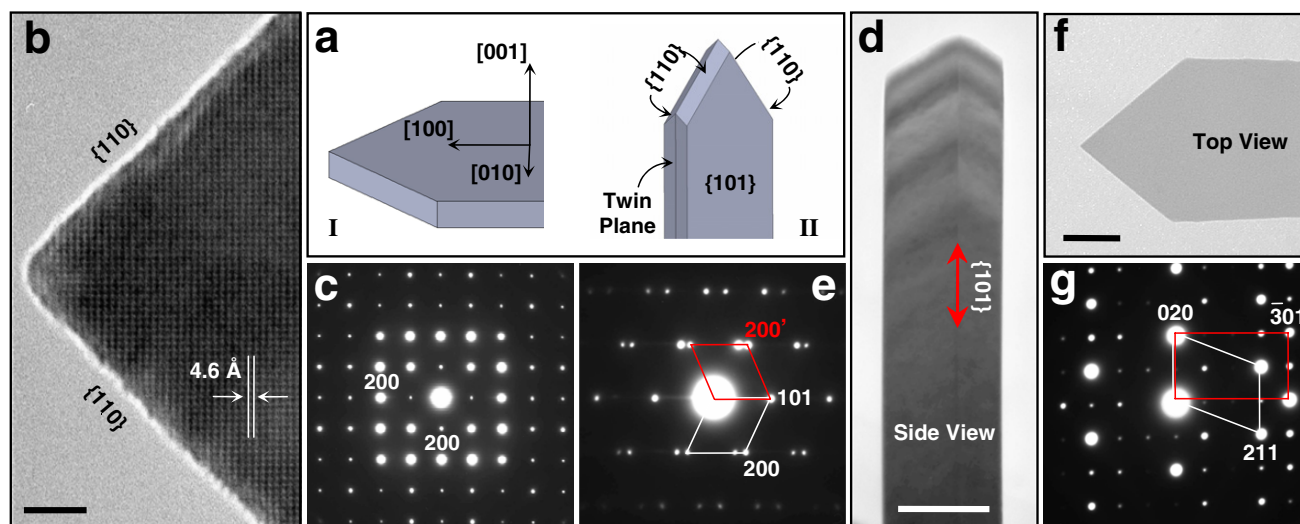


Figure 2. Detailed analysis of nanosword structure via TEM. (a) The orientation of the two types of nanoswords are shown schematically as type I and II. (b) HRTEM of type I nanosword grown along the [100] direction, with a large {001} facet, enclosed by two low energy {110} planes, and (c) the electron diffraction pattern along the [001] confirm the rutile phase. (d) Type II nanoswords enclosed by four {110} planes have a twin about the (101), as is evident from the electron diffraction pattern (e) along the side of the nanosword along the [100]. (f) Imaging the type II nanosword perpendicular to the broad {101} facet, the electron diffraction pattern in (g) shows the stacking of the [102] and [103] zones. Scale bars in (b), (d), and (f) are 4, 50, and 200 nm, respectively.

creating a tip angle of 114° . Its SAED pattern in figure 2(e) further confirms the twin structure, revealing that the twin plane belongs to a {101} plane. The top view of the type II nanosword, normal to the twin plane, is shown in figure 2(f), illustrating no visible evidence of the existence of the twin. However, the SAED pattern in figure 2(g) clearly shows two set of patterns from the top and bottom part of the twin, identified as the [102] and [103], respectively. The large top and bottom surfaces of these nanoswords belong to {101} planes, and its tip is terminated by four inclined {110} planes, creating an 80° taper angle. Greater detail about the TEM analysis may be found in the (supplementary data available at stacks.iop.org/Nano/21/485601/mmedia).

Figure 3 shows further nanosword characterization. The density of the nanoswords was observed to increase from $\sim 0.3 \mu\text{m}^{-2}$, $\sim 3.3 \mu\text{m}^{-2}$, and $\sim 4.7 \mu\text{m}^{-2}$ with increasing thickness of the evaporated titanium source layers from 1000 Å, 2000 Å, to 3500 Å, respectively, as shown in figures 3(a)–(c). The lengths and widths of the nanoswords for different times were measured via SEM, while thickness was measured using AFM. Figure 3(d) illustrates the expectedly normal distributions of the nanosword length, width, and thickness for a 10 min heating process, averaging $6.54 \mu\text{m}$, 542 nm, and 57.6 nm, respectively. Additionally, among a sampling of 120 nanoswords, 85% had sharp tips. A more complete representation of the time dependence of the nanosword dimensions is shown in figure 3(e). For each point, more than 50 nanoswords were imaged; error bars represent a single standard deviation. For growth substrates with a 2000 Å layer of source titanium, the resulting nanosword lengths and widths showed a linear dependence with growth time. The nanosword thickness showed a negligible time dependence, similar to the results obtained for nanobelts [17]. Finally, energy dispersive x-ray spectroscopy (EDS) via TEM

(JEOL 2010) was used to confirm the presence of the elements titanium and oxygen in the nanoswords. Greater detail on the characterization is offered in the (supplementary data available at stacks.iop.org/Nano/21/485601/mmedia).

For the rutile {101} and {001} facets (the broad surfaces of the nanoswords), there have been several experimental demonstrations of enhanced photoreactivity on these surfaces, including the oxidation of lead ions [27], reduction of silver [28], and evolution of ethane [29]. Likewise, theoretical studies have been reported that predict the dissociative adsorption of probe molecules [30] and reconstruction under ultrahigh vacuum [31, 32] on these higher energy surfaces, since they have a high density of undercoordinated surface titanium atoms [7].

The photocatalytic reactivity of nanoswords with broad {101} facets was compared to single crystalline (110) and (101) bulk rutile substrates by the quantitative photoreduction of silver [28]. A 365 nm lamp (UVP Mercury Pen-Ray) at power density of $\sim 7 \text{ mW cm}^{-2}$ (Coherent Fieldmate power meter) was used for the experiments. The results were then analyzed using tapping-mode atomic force microscopy to measure the volume of photoreduced silver on the surface.

Figure 4(a) illustrates a qualitative SEM comparison of the reactivity of the nanosword and (110) control substrate after 10 min exposure to UV, with the nanosword surface showing a much higher volume of photoreduced silver than the bulk reference (110) substrate. To validate the reaction, nanoswords were precisely positioned onto a perforated silicon nitride membrane window (SPI Supplies) [33], the photocatalytic reaction was allowed to occur, and the sample was imaged in a TEM, as shown in figure 4(b). The HRTEM image in figure 4(c) verifies a pure silver particle along the [110] zone axis, illustrating the d -spacing between {111} planes of 2.4 Å, and the EDS in figure 4(d) further validated the presence of elemental silver.

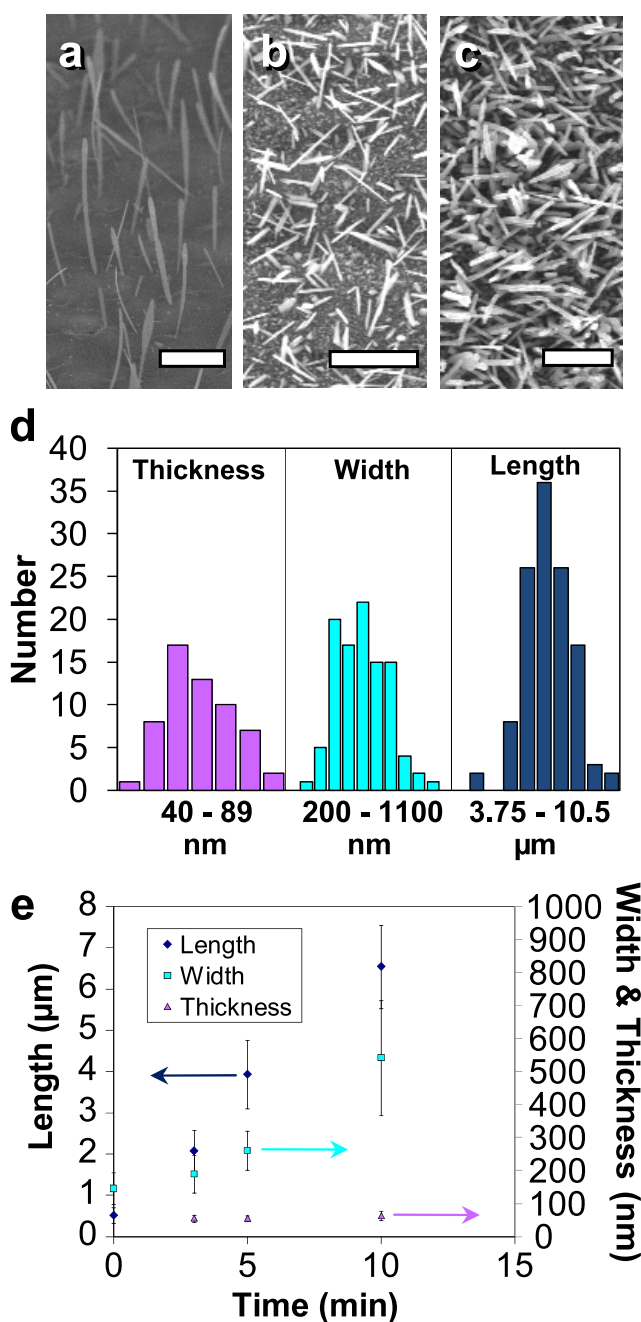


Figure 3. Additional nanosword characterizations. SEM images show that the density of the nanoswords depends on the initial titanium source material thickness, with 100, 200, and 350 nm shown in (a), (b), and (c), respectively. Distribution of characteristic dimensions (10 min synthesis), measured via SEM and AFM, were normal (d), and a time dependence of the length and width were approximately linear, with thickness varying negligibly for various synthesis times (e). All scale bars correspond to $2 \mu\text{m}$.

The quantitative comparison of nanoswords and substrates for various different times (1, 5, 10, 17, and 60 min UV exposure) is illustrated in figure 4(e). The data show that there was more than an order of magnitude increase in the photocatalytic activity of the nanoswords compared to the thermodynamically favorable (110) rutile reference surface. Furthermore, the nanoswords have a comparable yet higher reactivity than the (101) rutile reference, as expected, owing

to the similarity in the exposed facet. Another order of magnitude increase in the reactivity was obtained by exposing the nanoswords to a 15 s anneal in nitrogen/10% hydrogen at 800°C , which is believed to result from the increase in oxygen vacancies [34, 35] leading to a greater concentration of surface hydroxyls [36] necessary for the adsorption of silver ions [37]. The quantum efficiencies and reaction rates may be calculated from the experimental data in figure 4(e). For the measured illumination intensity of 1.3×10^{16} photons $\text{cm}^{-2} \text{s}^{-1}$, initial quantum efficiencies of 1.49, 0.42, 0.27, and 0.01% and reaction rates of 19.7, 5.6, 3.5, and $0.15 \text{ \AA min}^{-1}$ were observed for the hydrogen-treated nanoswords, unannealed nanoswords, control (101), and control (110) surfaces, respectively. Using the absorption coefficient for the rutile *c*-plane [38] and the mean nanosword thickness, initial quantum yields of 0.24 and 0.07 were estimated for hydrogen and unannealed nanoswords, respectively, which are comparable to previous reports for the rutile *c*-plane [39], but represents a lower limit due to unaccounted scattering effects.

3. Conclusion

In summary, we report the repeatable synthesis of a uniquely shaped, crystalline rutile TiO_2 nanostructure called a nanosword with a large percentage of highly reactive facets. Self-sourced and sans catalyst, the high quality nanoswords are large-scale synthesized in minutes, growing along low energy planes resulting in a large percentage of highly reactive facets and ultrasharp tips. Photocatalytic reactivity enhancements exceeding an order of magnitude were observed, and it is believed that such nanostructures could significantly improve the performance of a wide range of catalytic, clean-tech, and energy applications.

4. Methods

4.1. Nanosword synthesis

Substrates of titanium (99% pure, $500 \mu\text{m}$ -thick, acetone and isopropyl alcohol cleaned), copper (300 and 500 mesh TEM grids, Pacific Grid Tech), and heavily doped silicon ($0.002 \Omega \text{ cm}$, $550 \mu\text{m}$ -thick, piranha cleaned, p-type) were used for synthesis. Substrates were cut into $3 \times 3 \text{ mm}^2$ test specimen, and a 50–300 nm layer of 99.95% pure titanium was thermally evaporated ($5\text{--}7 \text{ \AA s}^{-1}$, $1\text{--}3 \times 10^{-6}$ Torr) onto them. The specimens were then mounted onto a ceramic chip holder, placed into a quartz synthesis chamber, and positioned approximately 6.5 mm below the center of an 8-turn, 12.7 mm inner-diameter, 3.25 mm pitch copper inductor (figure S1 available at stacks.iop.org/Nano/21/485601/mmedia). The system was sealed, evacuated, and purged with acetylene at 6 slpm at 50 Torr. Power was then initiated at 11.7 MHz, rapidly heating the growth substrate. The heat profile was monitored real-time via optical pyrometry with a spatial resolution of $\sim 20 \mu\text{m}$ along the axis of the coil, and the power was tuned *in situ* to obtain the desired heating profile (figure S2, supplementary data available at stacks.iop.org/Nano/21/485601/mmedia). Heating was sustained for several minutes, after which the system was vented and the specimen was inspected for nanoswords.

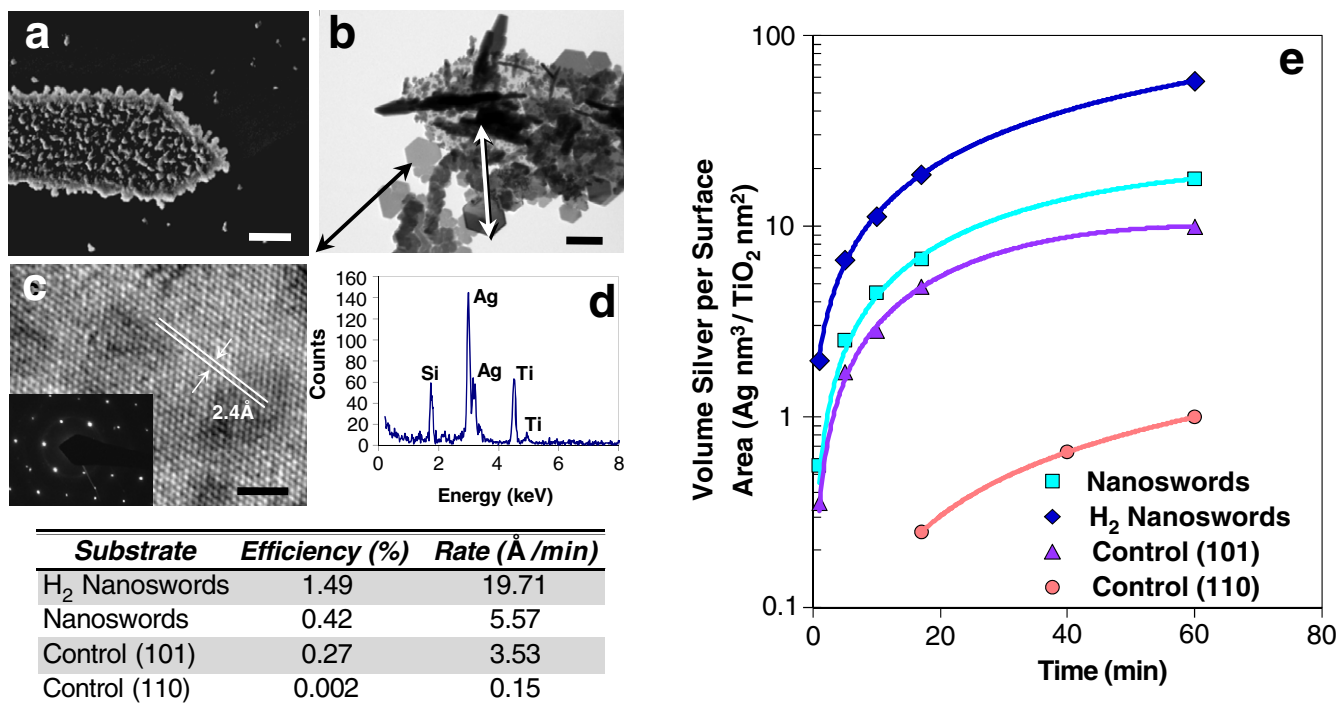


Figure 4. Nanosword photocatalytic reactivity testing. (a) Comparative reactivity of a nanosword and the (110) control substrate for a 10 min test, demonstrating a significantly larger volume of photoreduced silver of the broad nanosword facet. HRTEM of a photocatalytically reduced particle in (b) reveal a d -spacing of 2.4 \AA along the [110] zone in (c), and EDS in (d) confirm the particle is pure silver. The reactivity of the nanoswords in comparison to (110) and (101) control substrates is shown in (e). Standard error bars are calculated and shown in the (supplementary data available at stacks.iop.org/Nano/21/485601/mmedia). Scale bars in (a)–(c) are 200, 200, and 2 nm.

4.2. Photocatalytic substrate preparation

For photocatalytic experiments on nanoswords, $5 \times 5 \text{ mm}^2$ silicon with a 120 nm, MOS-quality, dry thermal oxide insulating layer was used as a support substrate. The substrates were diced, and nanoswords were positioned [33] onto the surface. Likewise, polished rutile $\text{TiO}_2(110)$ and (101) were purchased from MTI Corporation, the orientations were verified using XRD (Cu , $\lambda = 1.5418 \text{ \AA}$, figure S8 available at stacks.iop.org/Nano/21/485601/mmedia), and the specimens were cut into $1.5 \times 1.5 \text{ mm}^2$ substrates. All samples for photocatalytic testing were then placed in piranha solution (3:1 semiconductor grade sulfuric acid: 30% hydrogen peroxide) for 10 min, rinsed in deionized water, and dried in nitrogen. The substrates were then annealed in air for 1 h at 800°C [28], and all samples were subsequently cleaned in an oxygen plasma (1 min, 50 W, 100 sccm) before photocatalytic testing. Hydrogen-treated nanoswords were prepared by rapidly annealing nanoswords on oxidized silicon substrates for 15 s at 800°C in a nitrogen:hydrogen (90:10) environment. Samples were cooled to room temperature and followed with additional oxygen plasma cleaning before photocatalytic testing.

4.3. Photocatalytic testing

Samples were submerged in a glass petri dish with $\sim 8 \text{ ml}$ of 0.1 N standard silver nitrate solution (Acros Organics), and immediately isolated from ambient light. Power measurements

were taken for the ultraviolet light source (UVP mercury pen-ray, 365 nm) using a power meter (Coherent Fieldmate, 19 mm sensor aperture) while varying the sensor–light distance. A distance of 17 mm was set for photocatalytic testing where the lamp intensity was measured to be 7 mW cm^{-2} (figure S9 available at stacks.iop.org/Nano/21/485601/mmedia). The lamp was subsequently turned on, and each sample was exposed for a predesignated period of time. After each test, the samples were removed from the petri dish, rinsed in deionized water, and dried in nitrogen.

Acknowledgments

The authors acknowledge the contributions of T Kawano, L Luo, H Yang, L Folks, and H Kawayoshi. This project is supported in part by the DARPA N/MEMS Fundamental Sciences program. All test specimens for this work were fabricated in the UC Berkeley Microfabrication Laboratory.

References

- [1] Selloni A 2008 *Nat. Mater.* **7** 613–5
- [2] Yang H G, Sun C H, Qiao S Z, Zou J, Liu G, Smith S C, Cheng H M and Lu G Q 2008 *Nature* **453** 638–41
- [3] Diebold U 2003 *Surf. Sci. Rep.* **48** 53–229
- [4] Tian N, Zhou Z-Y, Sun S-G, Ding Y and Wang Z L 2007 *Science* **316** 732–5
- [5] Bikondoa O, Pang C L, Ithnin R, Muryn C A, Onishi H and Thornton G 2006 *Nat. Mater.* **5** 189–92

- [6] Gong X-Q and Selloni A 2005 *J. Phys. Chem. B* **109** 19560–2
- [7] Ramamoorthy M, Vanderbilt D and King-Smith R D 1994 *Phys. Rev. B* **49** 16721–7
- [8] Barnard A S and Curtiss L A 2005 *Nano Lett.* **5** 1261–6
- [9] Barnard A S, Zapol P and Curtiss L A 2005 *Surf. Sci.* **582** 173–88
- [10] Lazzeri M, Vittadini A and Selloni A 2001 *Phys. Rev. B* **63** 155409
- [11] Dai Y, Cogley C M, Zeng J, Sun Y and Xia Y 2009 *Nano Lett.* **9** 2455–9
- [12] Han X, Kuang Q, Jin M, Xie Z and Zheng L 2009 *J. Am. Chem. Soc.* **131** 3152–3
- [13] Pang Y and Wynblatt P 2006 *J. Am. Ceram. Soc.* **89** 666–71
- [14] Pan Z W, Dai Z R and Wang Z L 2001 *Science* **291** 1947–9
- [15] Wang Z L 2003 *Adv. Mater.* **15** 432–6
- [16] Sosnowchik B D, Lin L and Englander O 2010 *J. Appl. Phys.* **107** 051101
- [17] Dai Z R, Pan Z W and Wang Z L 2003 *Adv. Funct. Mater.* **13** 9–24
- [18] Kong X Y and Wang Z L 2003 *Nano Lett.* **3** 1625–31
- [19] Armstrong A R, Armstrong G, Canales J and Bruce P G 2004 *Angew. Chem. Int. Edn* **43** 2286–8
- [20] Lei Y, Zhang L D, Meng G W, Li G H, Zhang X Y, Liang C H, Chen W and Wang S X 2001 *Appl. Phys. Lett.* **78** 1125–7
- [21] Miao Z, Xu D, Ouyang J, Guo G, Zhao X and Tang Y 2002 *Nano Lett.* **2** 717–20
- [22] Kasuga T, Hiramatsu M, Hoson A, Sekino T and Niihara K 1999 *Adv. Mater.* **11** 1307–11
- [23] Peng X and Chen A 2006 *Adv. Funct. Mater.* **16** 1355–62
- [24] Wu J-M, Shih H C and Wu W-T 2005 *J. Vac. Sci. Technol. B* **23** 2122–6
- [25] Sosnowchik B D and Lin L 2006 *Appl. Phys. Lett.* **89** 193112
- [26] Luo L, Sosnowchik B D and Lin L 2007 *Appl. Phys. Lett.* **90** 093101
- [27] Ohno T, Sarukawa K and Matsumura M 2002 *New J. Chem.* **26** 1167–70
- [28] Lowekamp J B, Rohrer G S, Hostenpiller P A M, Bolt J D and Farneth W E 1998 *J. Phys. Chem. B* **102** 7323–7
- [29] Wilson J N and Idriss H 2002 *J. Am. Chem. Soc.* **124** 11284–5
- [30] Valentin C D, Tilocca A, Selloni A, Beck T J, Klust A, Batzill M, Losovyj Y and Diebold U 2005 *J. Am. Chem. Soc.* **127** 9895–903
- [31] Beck T J, Klust A, Batzill M, Diebold U, Valentin C D and Selloni A 2004 *Phys. Rev. Lett.* **93** 036104
- [32] Kubo T, Orita H and Nozoye H 2007 *J. Am. Chem. Soc.* **129** 10474–8
- [33] Sosnowchik B D, Chang J and Lin L 2010 *Appl. Phys. Lett.* **96** 153101
- [34] Shannon R D 1964 *J. Appl. Phys.* **35** 3414–6
- [35] Iwaki T, Komuro M, Hirosawa K and Miura M 1975 *J. Catal.* **39** 324–33
- [36] Schaub R, Thosttrup P, Lopez N, Laegsgaard E, Stensgaard I, Norskov J K and Besenbacher F 2001 *Phys. Rev. Lett.* **87** 266104
- [37] Herrmann J-M, Disdier J and Pichat P 1988 *J. Catal.* **113** 72–81
- [38] Jellison G E, Modine F A and Boatner L A 1997 *Opt. Lett.* **22** 1808–10
- [39] Hada H, Yonezawa Y, Ishino M and Tanemura H 1982 *J. Chem. Soc.-Faraday Trans.* **78** 2677–84